Materials Today Chemistry 29 (2023) 101394

Contents lists available at ScienceDirect

Materials Today Chemistry

journal homepage: www.journals.elsevier.com/materials-today-chemistry/

Soft nanostructures out of star-shaped triazines with flexible amide spacers: liquid crystals with a cubic to columnar transition with memory effect, gels and supramolecular chirality

A. Martínez-Bueno [a], R. Vidal [a], J. Ortega [b], J. Etxebarria [b], C.L. Folcia [b, ***], R. Giménez [a, **], T. Sierra [a, *]

[a] Instituto de Nanociencia y Materiales de Aragón (INMA), Departamento de Química Orgánica, Facultad de Ciencias, CSIC-Universidad de Zaragoza, 50009 Zaragoza, Spain
[b] Department of Physics, Faculty of Science and Technology, UPV/EHU, Bilbao, Spain

ARTICLE INFO

Article history:
Received 24 October 2022
Received in revised form
22 December 2022
Accepted 11 January 2023
Available online xxx

Keywords:
Tricarboxamides
Hexagonal columnar
Cubic micellar
Organogels
Chiroptical properties

ABSTRACT

This work reports the synthesis and characterization of a new family of star-shaped tricarboxamides with C_3-symmetry that have flexible amide spacers linking a tris(triazolyl)triazine core with three trialkoxyphenyl groups. The presence of amide groups allows the formation of intermolecular hydrogen bonds that reinforce π-stacking and van der Waals interactions, promoting liquid crystalline behavior, and self-assembly in solvents leading to organogels. As determined by polarized optical microscopy, differential scanning calorimetry and X-ray diffraction on powder samples, all the three reported molecules present a hexagonal columnar (Col_h) phase stable at room temperature. Interestingly, they show a transition to a cubic micellar mesophase (BCC) at high temperatures. A mechanism for this transition, which is consistent with the fragmentation of columns to form supramolecular spheres, was elucidated from X-ray studies on aligned samples. Moreover, on cooling from the BCC to the columnar phase a preferential orientation of columns occurs, according to which each cubic domain gives rise to four hexagonal domains. The ability of the synthesized structures to aggregate in solvent media was studied in a variety of organic solvents, and all of them were able to gel 1-octanol at low concentrations. X-ray studies of gels and xerogels were carried out and showed a molecular organization consistent with Col_h order. FTIR studies were carried out to analyze the formation of hydrogen bonds and the influence of the length of the flexible spacer in the liquid crystalline state and in the organogels. Furthermore, the presence of a stereogenic center in the flexible amide spacer leads to macroscopic chirality in the liquid crystal state and the organogels in 1-octanol as demonstrated by circular dichroism spectroscopy.

1. Introduction

In the search for advanced materials, the bottom-up fabrication of soft nanostructures relies on the design of molecules that encode their ability to self-assemble either onto surfaces, in bulk or in solvents [1].

An important class of soft materials are those consisting of stacks of molecules, due to their potential to obtain one-dimensional (1D) materials for electronic and optical applications [2–4]. In this respect, columnar liquid crystals made of discotic molecules are widely explored [5]. Out of this classical shape, a versatile molecular structure to regulate liquid crystalline assemblies is the three-arm star-shape, which consists of an aromatic ring (usually benzene or triazine) linked to three arms in a C_3-symmetry [6,7]. Their tunable molecular design allows a precise control of the internal architecture since the nature of the core and the arms can modify the intermolecular interactions that dictate the self-assembly of the building blocks, and hence their properties [8–14].

In order to stabilize molecule stacks, one of the most efficient way is to include functional groups that allow intermolecular/intracolumnar hydrogen bonds (H-bonds) to reinforce π-stacking and van der Waals interactions between mesogens [15,16]. This is especially interesting for C_3-symmetric molecules since this structure gives the possibility of including three amide groups to get a triple-decker H-bonding self-complementary mesogen. In this

* Corresponding author.
** Corresponding author.
*** Corresponding author.
E-mail addresses: cesar.folcia@ehu.es (C.L. Folcia), rgimenez@unizar.es (R. Giménez), t.sierra@csic.es, tsierra@unizar.es (T. Sierra).

https://doi.org/10.1016/j.mtchem.2023.101394

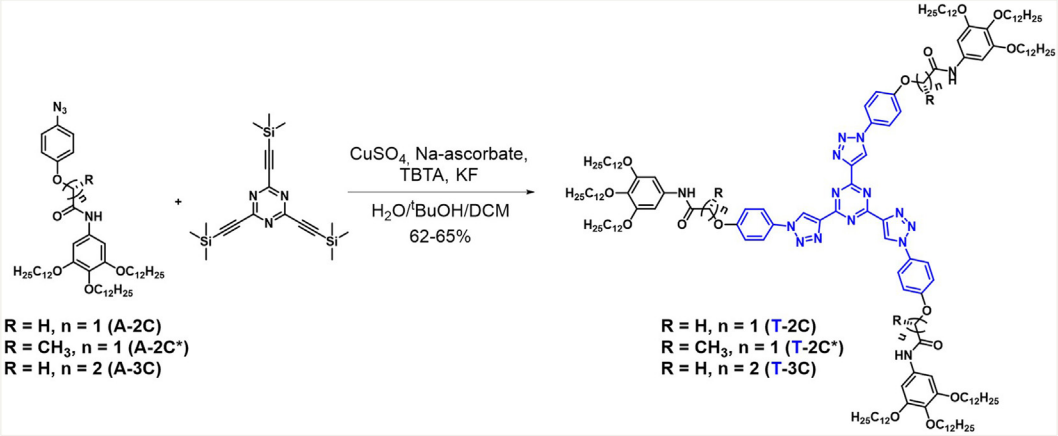

Scheme 1. Synthesis of the star shaped trisamide molecules.

respect, 1,3,5-benzenetricarboxamide derivatives are paradigmatic examples that form supramolecular stacks [17]. Moreover, they help to form helical 1D aggregates dictated by three-fold α-helix-type intermolecular H-bonds, and this amplifies the molecular chirality [18]. Other star-shaped cores, among them oligo(phenylene ethynylene) [19], 1,3,5-triphenylbenzene [20] or triphenylamine [21], have also been modified with amide moieties in order to get tricarboxamides with helical organizations in the liquid crystal state and in solvents.

The reported systems contain the amide group directly attached to the aromatic core, and the use of aliphatic spacers between the core and the arms has been barely explored [22]. Nevertheless, aliphatic amide spacers in the arm would permit segregating different functional moieties in the mesophase. Thus, in a different context, Aida and co-workers found that by using flexible amide spacers with different length in 4,5-dithiaphtalonitrile fan-shaped molecules dramatically changed either the liquid crystalline or the ferroelectric properties due to a better formation of amide H-bonds [23].

In this work we report a new family of C_3-symmetric star-shaped tricarboxamides having flexible amide spacers attached to a tris(triazolyl)triazine (T) core [24] (Scheme 1). This core, known by its tendency to show columnar LC behavior leading to 1D functional nanostructures, is a promising candidate to explore new self-assembled architectures, both in the LC state [8] and upon aggregation in solvents [25]. The amide groups are included within flexible and chiral spacers, whose length has a significant influence in the formation of intermolecular H-bonds and therefore in the self-assembly properties. We here show the synthesis and characterization of tris(triazolyl)triazines symmetrically functionalized with trialkoxyphenyl groups using three different flexible amide spacers, and the study of their self-assembly in bulk and in solvents.

All compounds are liquid crystals and exhibit hexagonal columnar phases at room temperature. Unexpectedly, they show a transition to a cubic micellar mesophase (BCC type) at high temperatures, which means the change from a 1D type nanostructure to a 0D nanostructure. Up to our knowledge, this phase behavior is unprecedented in star-shaped systems. Only two cases report a single cubic phase for star-shaped systems, one is a dendronized tricarboxamide [26], and the second a non-symmetric star-shaped oligobenzoate [27]. An XRD study in oriented samples has helped to elucidate the mechanism for the columnar-to-cubic-to-columnar transition [28,29]. The transference of the chirality from the molecule to the columns and the supramolecular spheres was studied by circular dichroism (CD). The results evidence that molecular packing is similar in both mesophases and therefore the formation of the supramolecular spheres could be mediated by a fragmentation of the columns [30].

It has been recognized the interest on molecules that show thermotropic liquid crystalline behavior and are also able to self-assemble in solution with an internal molecular order similar to that of the mesophase [31]. Different molecular structures have been reported to show this dual behavior [11,32–36]. In this respect, the ability of the synthesized structures to aggregate in solvent media was studied in organic solvents of different nature. Surprisingly, all these compounds were able to gel 1-octanol at low concentrations without disturbing intermolecular H-bonds between amides. The transference of the chirality from the molecule to the gel fibers was also studied by CD, observing higher transference than in the mesophase.

2. Results and discussion

2.1. Synthesis

Star-shaped trisamide molecules, **T-2C**, **T-2C*** and **T-3C**, were synthesized from aromatic azides by adapting the previously described procedure consisting in a *one-pot* triple deprotection-triple copper-catalyzed azide-alkyne cycloaddition (CuACC) of 2,4,6-tris[(trimethylsilyl)ethynyl]-1,3,5-triazine (Scheme 1) [24]. In the present work, the one-pot reaction was optimized taking into account another procedure described in the literature for CuAAC reactions with 2,4,6-triethynyl-1,3,5-triazine [37]. Thus, the reaction was performed in a biphasic mixture of dichloromethane/*tert*-butanol/water (8/2/1) using tris[(1-benzyl-4-triazolyl)methyl] amine (TBTA) as chelating agent and potassium fluoride as deprotection reagent. After stirring overnight, full conversion was obtained without byproducts, as it was observed by ^{1}H NMR, and the isolated yields of the one-pot reaction were improved, up to 65%. All experimental details and characterization data are collected in the Supporting Information.

The precursory azides (**A-2C**, **A-2C*** and **A-3C**) were synthesized through an amidation reaction between azide-containing carboxylic acids **8**, **9** or **10** and 3,4,5-tridodecyloxyaniline **3** (Scheme 2).

Compound **3** was synthesized starting with the alkylation of pyrogallol with 1-bromododecane **1**, the subsequent nitration and the reduction of 1,2,3-dodecyloxy-5-nitrobenzene (**2**) [38].

Azide-containing carboxylic acids **8**, **9** and **10** were prepared from *p*-azidophenol [39] or *p*-nitrophenol, following different strategies depending on the length of the flexible spacer. Compound **8** was synthesized from *p*-azidophenol by a Williamson etherification with ethyl α-bromoacetate and subsequent

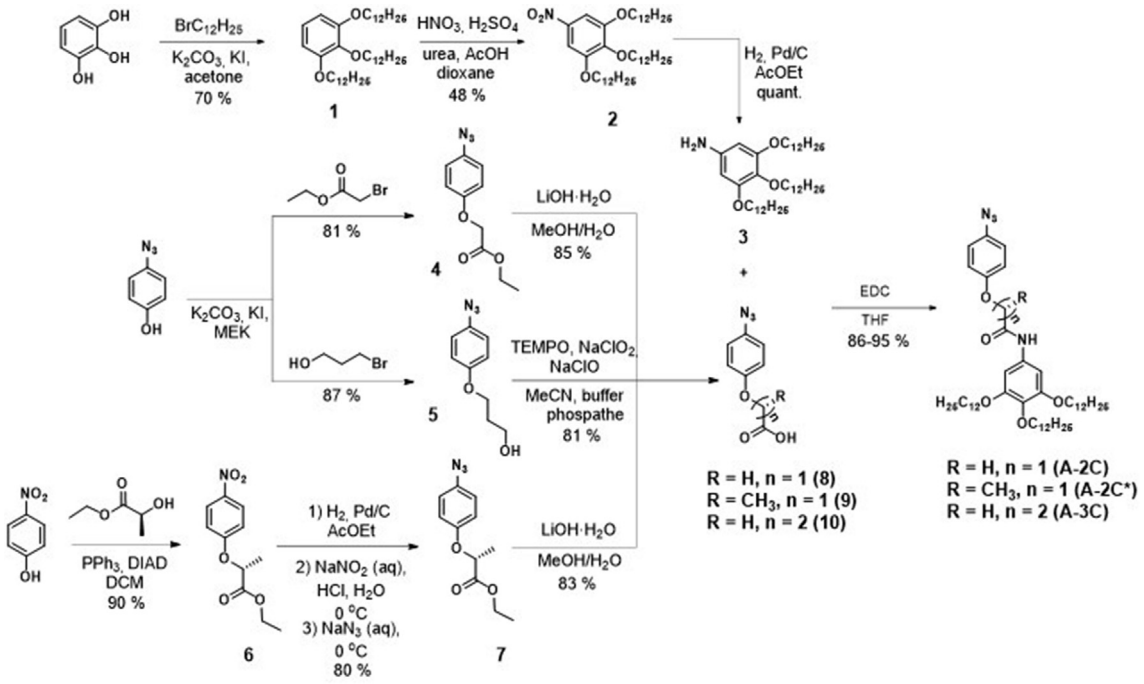

Scheme 2. Synthesis of the precursory aromatic azides.

hydrolysis of the ester to carboxylic acid. In order to prepare the three-carbon length spacer precursor **10**, the coupling of *p*-azidophenol with β-bromopropionic acid through a Williamson reaction was not possible due to α,β-elimination under these conditions. In order to avoid this, 3-bromopropanol was first introduced under Williamson conditions to yield intermediate **5**. The subsequent oxidation of the terminal CH_2OH group with (2,2,6,6-tetramethylpiperidin-1-yl)oxidanyl (TEMPO) and bleach [40] afforded the carboxylic acid **10** in good yields. Compound **9** was prepared by a Mitsunobu etherification between *p*-nitrophenol and (S)-(−)-ethyl lactate. *p*-Azidophenol was avoided because of the reduction of the azide group in the presence of triphenylphosphine [41]. The hydrogenation of the nitro group and the diazotization of the resulting aniline in the presence of NaN_3 yielded the azide **7**, which was hydrolyzed to the acid **9**.

2.2. Liquid crystalline behavior

2.2.1. Thermal properties

All compounds display liquid crystalline phases in broad temperature ranges. Thermal behavior and liquid crystalline properties listed in Table 1 were determined by different characterization techniques, namely polarized optical microscopy (POM), thermogravimetric analysis (TGA), differential scanning calorimetry (DSC) and X-ray diffraction (XRD).

Table 1
Thermal and liquid crystalline properties of the final compounds.

Compound	Thermal properties[a] (T °C, [ΔH kJ/mol])	$T_{5\%}$ [b]
T-2C	Col_h 80[c] BCC 204[d] [11] M[e] 231 [2.2][f] I	350
T-2C*	Col_h 90[c] BCC 158 [0.9] I	338
T-3C	Col_h 131 [6.7] BCC 216 [3.8][f] I	342

[a] Temperatures and enthalpies from second heating scan of DSC termogram at a heating rate of 10 °C min^{-1}, onset temperatures unless otherwise noted.
[b] Temperature corresponding to a 5% weight loss by TGA.
[c] XRD and POM data.
[d] Transition temperature taken at the maximum of the peak.
[e] Unidentified mesophase.
[f] Data from first heating scan. Col_h: Hexagonal columnar mesophase; BCC: Body centered cubic mesophase.

In POM observations, pristine samples of **T-2C** and **T-2C*** exhibited birefringence at room temperature (Fig. 1a and Fig. S9a). On heating, birefringence started to disappear slowly at around 80–90 °C and the samples became optically isotropic (Fig. S9b), what was consistent with the transition to a BCC phase (see XRD studies). At this point, it was possible to observe birefringence when mechanical stress was applied (Fig. 1b), but it disappeared when the pressure was released. On cooling down from the isotropic liquid, none of the materials showed birefringence (Fig. 1c) unless mechanical stress was applied. Below 80 °C, a slightly birefringent texture was formed (Fig. 1d and Fig. S9c) indicating the transition to the Col_h, which remained stable at room temperature.

T-3C was obtained as a crystalline solid (Fig. S9d) that in the first heating scan became optically isotropic at 155 °C. Above that temperature, birefringence was only observed under mechanical stress up to 216 °C. This was consistent with the formation of a BCC phase (see XRD studies), as it was found for **T-2C** and **T-2C***. On cooling (Figs. S9e–f), the transition from the BCC phase to a Col_h phase was detected by the appearance of birefringence at 120 °C. The texture of the Col_h phase remained stable at room temperature and transformed into the optically isotropic texture of the BCC phase on heating above 131 °C. No crystallization was observed in subsequent heating-cooling cycles.

Although **T-2C** and **T-3C** showed TGA thermograms with 5% weight loss temperature over 335 °C, much higher than the clearing point, when both compounds were heated close to the clearing point some orange spots appeared in the samples, likely indicating some decomposition processes without volatile formation in the transition to the isotropic liquid. DSC thermograms corresponding to the first and second heating processes were not the same; a slight reduction of the clearing temperature was observed (Fig. S10 and Fig. S12). This partial decomposition was taken into account for data characterization (Table 1) and during thermal treatments for XRD studies.

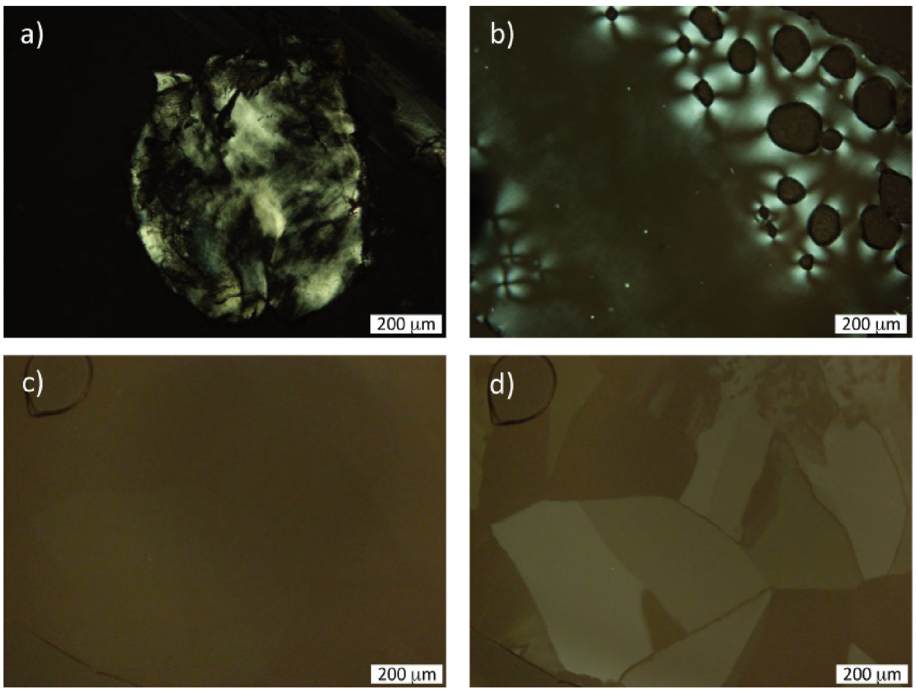

Fig. 1. Photomicrographs of textures observed by POM for **T-2C** at (a) pristine sample at room temperature, (b) 130 °C on heating, under mechanical stress, (c) 170 °C on cooling from the isotropic liquid and (d) room temperature on cooling from the isotropic liquid.

The first heating thermogram of compound **T-2C** shows three broad transitions before the transition to the isotropic liquid, with respective maximum temperatures around 70 °C, 160 °C and 204 °C (Fig. S10a). Only the latter reappears in the first-cooling scan, indicating that transitions at 70 °C and 160 °C are due to partial crystalline nature of the pristine sample. According to POM observations, and confirmed by XRD studies (see below), the transition from Col_h to BCC phase does not show a peak in the thermograms. Furthermore, the transition observed at 204 °C corresponds to the transition from the BCC phase to an upper temperature phase (M), which could not be identified. The presence of a branched spacer, which hinders intermolecular interactions, makes compound **T-2C*** to show lower clearing point than its achiral analogue, and it does not decompose in the isotropic phase (Fig. S11). In this case, in the second heating cycle, only the transition to the isotropic liquid is observed at 158 °C. However, no clear peak is observed to be assigned to the transition between the BCC and Col_h phases as detected by POM and measured by XRD (see XRD studies).

In contrast to their analogues, compound **T-3C** exhibits an endothermic peak at 131 °C during the second heating scan, which corresponds to the transition from the Col_h to the BCC phase.

2.2.2. Mesophase structure

2.2.2.1. XRD studies in powder samples. The mesomorphic behaviour of all the three compounds was confirmed by XRD experiments at different temperatures in samples cooled from the isotropic (**T-2C***) or treated at 200 °C (**T-2C** and **T-3C**). The structural details of the phase above 210 °C of compound **T-2C** could not be studied by XRD because at this temperature the sample is unstable during the time necessary to perform XRD experiments. XRD data and structural parameters are summarized in Table 2.

At room temperature, the XRD pattern of **T-2C** contains two small angle reflections due to distances related with a ratio of 1:1/$\sqrt{3}$ (Fig. 2a and Fig. S13a), which correspond to the indices (100) and (110) of a hexagonal lattice. In the high angle region, a diffuse halo at 4.5 Å characteristic of the liquid crystal state is detected, in addition to an outermost sharp reflection at 3.4 Å, which indicates a well-defined periodicity of the structure along the direction of the columnar axis. The XRD pattern of compound **T-2C*** at room

Table 2
X-ray diffraction data.

Compound	T (°C)	Mesophase	Lattice parameters	d_{obs}(Å)	d_{calc}(Å)	Miller indices (hkl)
T-2C	rt	**Col_h**	$a = 42.9$ Å	37.2	37.2	100
			$c = 3.4$ Å	21.5	21.5	110
				4.5 (dif)		
				3.4		001
	170	**BCC**	$a_c = 53.6$ Å	37.9	37.9	110
				26.7	26.8	200
				21.9	21.9	211
				19	19	220
				4.5 (dif)		
T-2C*	rt	**Col_h**	$a = 42.2$ Å	36.5	36.5	100
				21	21.1	110
				4.5 (dif)		
	150	**BCC**	$a_c = 49.9$ Å	35.2	35.3	110
				24.7	24.9	200
				20.6	20.4	211
				4.5 (dif)		
T-3C	rt	**Col_h**	$a = 45.5$ Å	39.4	39.4	100
				22.9	22.7	110
				4.5 (dif)		
	180	**BCC**	$a_c = 58$ Å	41.1	41.0	110
				29	29	200
				23.5	23.7	211
				20.6	20.5	220
				15.5	15.5	321
				4.5 (dif)		

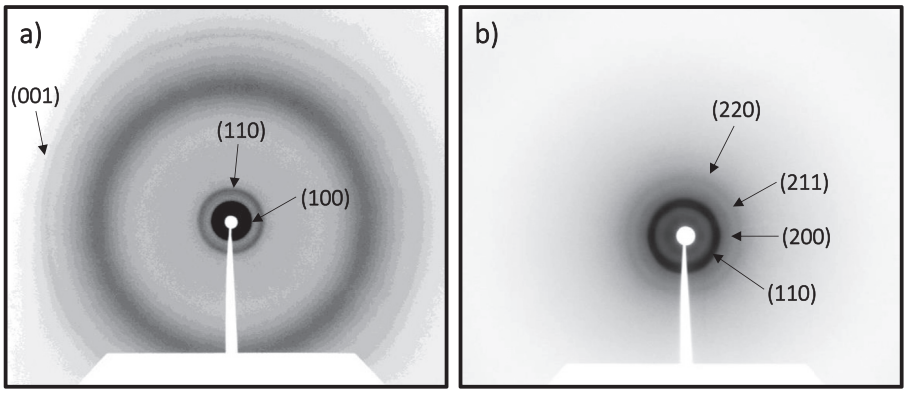

Fig. 2. X-ray diffractograms of compound **T-2C** at room temperature (a) and 170 °C (b).

temperature exhibits the reflections (100) and (110) of the hexagonal lattice and the broad halo of the liquid crystalline state (Fig. S14a). For compound **T-3C**, the reflections (100) and (110) of a hexagonal lattice were also observed in the small angle region (Fig. S15a). Neither **T-2C*** nor **T-3C** showed a reflection at high angles related with a well-defined periodicity of the structure along the direction of the columnar axis.

The number of molecules per unit cell (Z) in the Col_h phase was calculated for all the three compounds considering that the density (ρ) of the materials can be estimated by the equation $\rho = (M{\cdot}Z)/(N_A{.}V)$, where M is the molar mass; Z is the number of molecules per disk; N_A is Avogadro's number and V is the volume of the unit cell calculated with measured XRD parameters ($V = a^2{\cdot}\sqrt{3}/2{\cdot}c$). For **T-2C** a parameter $c = 3.4$ Å was measured from the XRD pattern. For compounds **T-2C*** and **T-3C**, which didn't show the corresponding reflection, this parameter was assumed as $c = 3.4$ Å, by analogy to **T-2C**. A density value of 0.91 g/cm^3 was experimentally estimated by buoyancy method by using mixtures of H_2O/MeOH (see SI) [12]. According to these parameters a $Z = 1$ value was estimated for all the three compounds, indicating one molecule per stacking unit (see calculation details in the supporting information).

XRD experiments at different temperatures were carried out according to the DSC thermograms. When compounds **T-2C** and **T-2C*** were heated above 80 °C and 90 °C, respectively, two additional reflections appeared in the small angle region that corresponded to a distance ratio $1{:}1/\sqrt{2}{:}1/\sqrt{4}$ (Fig. 2b, Fig. S13b and Fig. S14b). Furthermore, the reflections in the low angle region exhibited higher intensity and definition. However, the external sharp reflection due to the periodic stacking, which was present in the room temperature XRD pattern of compound **T-2C,** disappeared after this transition. When compound **T-3C** was heated above 136 °C, three additional reflections appear in the small angle in a relationship $1/\sqrt{2}$, $1/\sqrt{4}$ and $1/\sqrt{7}$ with respect to the main reflection (Table 2, Fig. S15b). This set of indices is only feasible for a micellar BCC phase whose possible $1/d^2$ values are in the ratio 1:2:3:4:5:6:7 [42]. The cubic symmetry explains the extinction between crossed-polarizers of all compounds during the heating process, although after applying mechanical stress birefringence appeared, probably due to a field-induced effect. Similar behavior was described for nonsymmetrical star-shaped oligobenzoates that self-assembled into spherical micelles adopting a cone-shaped conformation by folding the arms [27]. In the present case, since the C_3-symmetric tris(trazolyl)triazine core is nearly planar [43], such folding should occur at the flexible spacer containing the amide group. It is proposed that the aniline-derived groups can situate at different heights with respect to the plane defined by the core (Fig. 3a and b). Accordingly, the formation of spherical micelles can be explained by the division of the columns into small fragments constituted by such different folded-conformers of the molecule that arrange in spherical assemblies [26]. A schematic representation for **T-2C*** is shown in Fig. 3c.

The number of molecules per unit cell in the BCC mesophase was calculated by equation $Z = a_c^3/V$, where V, as defined above, is the volume of the hexagonal unit cell containing one molecule and a_c the cell parameter of the cubic phase [27]. The same density value ($\rho \approx 0.91$ g/cm^3) that in the columnar mesophase was assumed to estimate the molecular volume (see calculation details in the supporting information). For **T-2C**, around 32 molecules form the unit cell, and considering that there are two micelles per unit cell, the number of molecules per micelle is around 16. For the chiral analogue **T-2C*,** a number of 26 molecules was obtained for the unit cell, being lower probably because the steric hindrance of the branched spacer makes the molecular volume bigger. However, for compound **T-3C**, this number was estimated to be 40 molecules. In this case the unit cell is larger, as expected, since the molecule has a longer spacer.

2.2.2.2. XRD studies in partially aligned samples. In order to obtain more information about the structural characteristics of the materials, we tried to obtain certain degree of alignment in the samples. With this idea, measurements were performed in the Col_h and BCC phases of compounds **T-2C** and **T-3C** after subjecting them to uniaxial stress along the capillary axis at room temperature. The samples were subsequently heated to the BCC phase and finally cooled again to the hexagonal phase. After this treatment, XRD experiments revealed that in fact a partial alignment was achieved, since the circular rings of the X-ray reflections, characteristic of powder samples changed to an almost hexagonal distribution of discrete points at each corresponding Bragg angle. This pseudo-hexagonal distribution remained unaltered at both Col_h and BCC phases upon subsequent thermal cycling. We will try to explain the obtained results next.

To discuss these ideas we should first note that in general, in a low-angle XRD experiment, a particular (hkl) reflection is observable when the corresponding reciprocal vector is perpendicular to the incident X-ray beam. Starting with the cubic phase, it is well known that the reciprocal lattice of a BCC lattice of cell parameter a, is a cubic FCC lattice of parameter $2/a$. In our case, the hypothesis is that at room temperature the stress produces randomly oriented hexagonal domains with a common hexagonal axis [001] along the capillary axis and, on heating to the BCC phase, the capillary axis becomes parallel to the cubic [111] direction. Thus, after the alignment treatment and subsequent heating, the sample is constituted by cubic domains sharing the [111] direction (capillary axis), and are related to each other by arbitrary rotations φ about that axis. The X-ray beam is along a direction perpendicular to [111]. As can be seen in

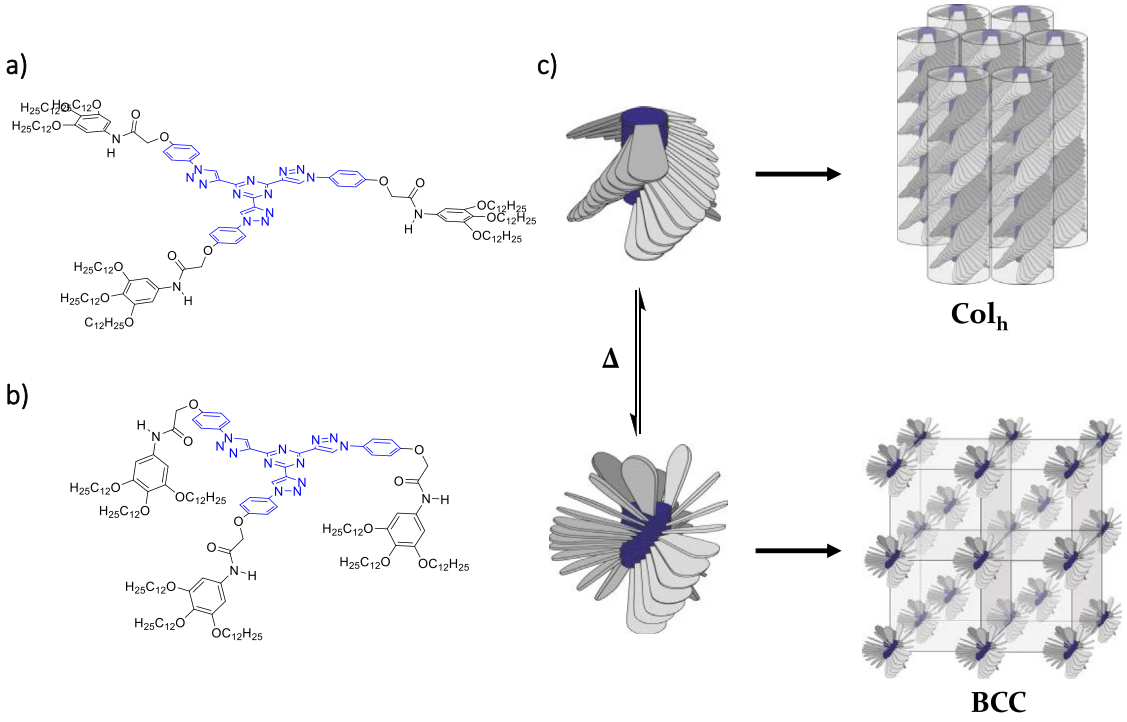

Fig. 3. Representation of **T-2C** conformers with the arms in the plane of the core (a), perpendicular to the core (b) and a schematic representation of the formation of the columnar and the BCC mesophases for T-2C* (c).

Fig. 4, there is always a φ angle for which any point of the reciprocal lattice will give rise to diffraction. On a two-dimensional detector, a diffraction peak (*hkl*) is then observed in a direction that makes an angle α with the meridian equal to the angle between the reciprocal vector (*hkl*) and the [111] direction (Fig. 4).

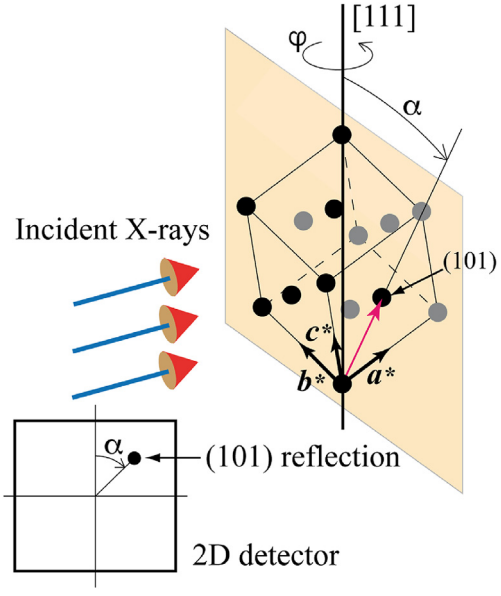

Fig. 4. Scheme of the diffraction experiment for the BCC phase. The set of domains sharing the [111] direction is equivalent to a single crystal that rotates continuously about that direction. A reflection is observed on the detector whenever a point of the FCC reciprocal lattice (black and grey circles) crosses the (orange) plane perpendicular to the incident X-ray beam.

Table 3
Angles between the diffraction directions and the capillary axis for the different groups of (*hkl*) reflections. Each (*hkl*) group contains all the reciprocal vectors obtained by permutations and sign changes of the Miller indices that keep constant the modulus of the (*hkl*) vector $\sqrt{h^2+k^2+l^2}$.

Angles with meridian α	Prototype reflection (*hkl*)	$\sqrt{h^2+k^2+l^2}$
± 35.3°, ± 144.7°, ± 90°	(110)	$\sqrt{2}$
± 54.7°, ± 125.3°	(200)	$\sqrt{4}$
± 19.5°, ± 160.5°, ± 61.9°, ± 118.1°, ± 90°	(211)	$\sqrt{6}$
± 35.3°, ± 144.7°, ± 90°	(220)	$\sqrt{8}$

Analytically, α can be computed through the scalar product of the reciprocal vector and the unit vector along [111]. We easily arrive at the expression:

$$\cos\alpha = \frac{h+k+l}{\sqrt{3}\,\sqrt{h^2+k^2+l^2}}$$

The angles for the first reciprocal vectors are shown in Table 3. The distance from the center of the diagram to the (*hkl*) peak is proportional to the modulus of the reciprocal vector $\sqrt{h^2+k^2+l^2}$. The resulting diffraction pattern is schematized in Fig. 5a, and the experimental results for compound **T-2C** are shown in Fig. 5c. Note that the diagram does not have perfect 6-fold symmetry even if we restrict ourselves to the innermost (and usually strongest) (110)-type reflections. This is in contrast with some claims made in several reports [29,44,45]. Certainly, the hexagon formed by the (110) group of reflections is close to being regular but, in fact, it is not. It can be easily checked that the two sides of the hexagon perpendicular to the capillary are slightly larger.

On cooling from the BCC phase, the Col$_h$ phase is reached. We will now show that the result in the Col$_h$ phase can be explained with the idea that each cubic domain gives rise to four hexagonal

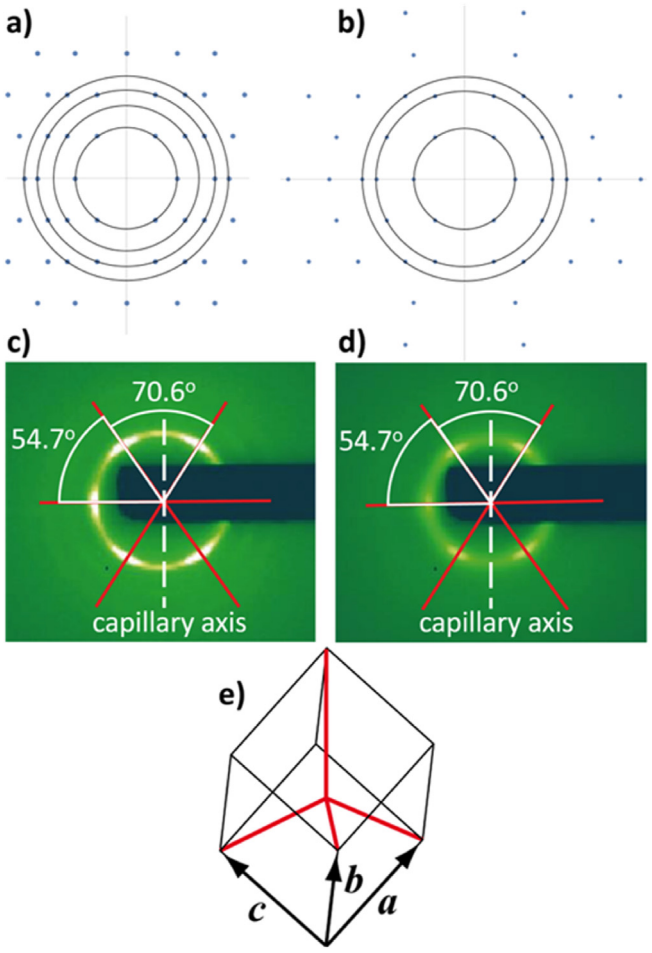

Fig. 5. Scheme of the 2D X-ray diffraction pattern obtained in the vertically oriented capillary. a) Cubic phase: Circles group reflections with the same (*hkl*) modulus, whose α values are indicated in Table 3 b) Hexagonal phase obtained on cooling from the cubic phase: The three circles group the (10), (11) and (20)-type reflections. Further reflections at wider angles are also shown. 2D X-ray diffraction pattern of the cubic (c) and the hexagonal phases (d) of compound **T-2C** with the theoretical angles of the hexagon formed by the (110) and (10) groups of reflections respectively. (e) Relative orientation of the cubic axes in the BCC phase and the four possible hexagonal axes arising on cooling (red lines).

domains whose axes are oriented in tetrahedral directions along the four diagonals of the cube. The domain structure in the capillary is now more complicated than in the above structure, and the calculation of the diffraction pattern is more involved. Similarly to the cubic phase, there are domains related by φ rotations about the capillary axis ([001] hexagonal direction). But for each of them, there are 3 possible additional domains obtained by rotations of 109.5° (arccos(1/3)) about the reciprocal vectors (10), $(\bar{1}1)$ and $(0\bar{1})$ of the hexagonal lattice (Fig. 6). In these domains the hexagonal axis is along the directions labeled as 1,2 and 3 in Fig. 6, which coincide with the cubic $[11\bar{1}]$, $[1\bar{1}1]$ and $[\bar{1}11]$ directions of the parent phase (see Fig. 5e). The final scheme of XRD pattern is shown in Fig. 5b. The experimental results for **T-2C** and **T-3C** are shown in Fig. 5d, Fig. S16 and Fig. S17. The result is quite similar to that of the cubic phase. This happens because of the peculiar relationship of orientations between the four hexagonal domains coming from each cubic domain, with the 4 hexagonal axes parallel to the 4 diagonals of the cube (Fig. 5e). In the hexagonal phase, the (10), (11) and (20)-type reflections play the role of the cubic (110), (211) and (220)-type peaks. The most remarkable difference is the absence of diffraction for the counterparts of the cubic (200)-type reflections.

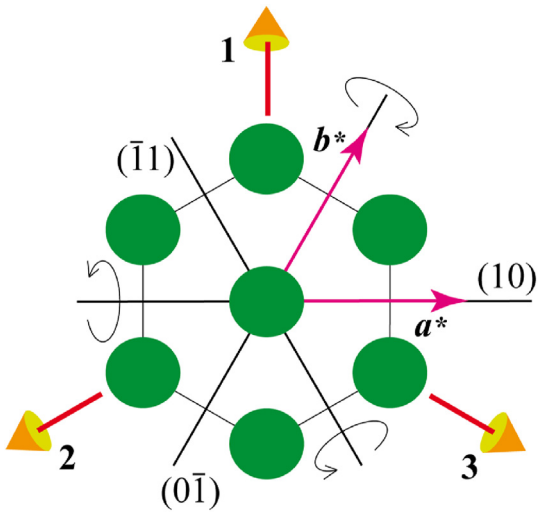

Fig. 6. View along the capillary axis of one of the four hexagonal domains. The columns point towards the reader and are represented by green circles. The reciprocal basis (***a****, ***b****) is also represented. The other three hexagonal domains, whose axes are oriented along the directions **1**, **2**, and **3**, are obtained from rotations of 109.5° about the (10), $(\bar{1}1)$ and $(0\bar{1})$ reciprocal directions as shown.

Similar X-ray patterns have been reported by Percec and coworkers in some mesophases of materials made of dendritic molecules, which can form columns or supramolecular spheres by adopting a crown-shape conformation [29,44,45]. The persistence of the observed patterns on thermal cycling was named supramolecular orientational memory (SOM). SOM occurs after cooling an oriented cubic phase which gives rise to the formation of columnar hexagonal domains where the hexagonal axes are oriented along symmetry-equivalent directions of the cubic phase. This preferential orientation of the columns is caused by a closer contact of the spheres in some specific directions of the cubic lattice. The process can be repeated indefinitely by heating and cooling across the transition, and can only be erased if the material is heated into the isotropic phase. This phenomenon was also studied in dendritic molecules that form supramolecular spheres by adopting a conic-shape [46]. However, SOM effect has not been reported in star-shaped systems before.

2.2.2.3. FTIR studies of intermolecular H-bonds. In order to study the presence of intermolecular hydrogen bonds either in the columnar or in the cubic mesophases, infrared spectroscopy experiments at variable temperature were carried out. At room temperature, compounds **T-2C** (Fig. S18) and **T-2C*** (Fig. 7a) show a broad N-Hst band centered around 3320 cm^{-1}, consistent with the H-bond N—H—O=C, and one additional band around 3410 cm^{-1}, which corresponds to free N—H [47]. As the temperature increases, the associated amide band decreases and shifts to higher wavenumbers whereas non-associated amide band rises gradually. In addition, the C=Ost band appeared as a broad band between 1650 and 1730 cm^{-1}, likely due to the overlapping of bands corresponding to associated and non-associated carbonyl groups. Also, this band is gradually shifted to higher wavenumbers when increasing the temperature due to weaker hydrogen bonded interactions. On the other hand, compound **T-3C** shows only one N-Hst band (Fig. 7b) centered at 3300 cm^{-1} and a C=Ost band centered around 1660 cm^{-1} with a shoulder at 1690 cm^{-1}. This is in agreement with a higher association degree through hydrogen bonds in comparison with **T-2C** and **T-2C***. In this case, when the temperature increases, the same tendency was observed, i.e. associated N-Hst and C=Ost bands show intensity reduction and gradual shift to

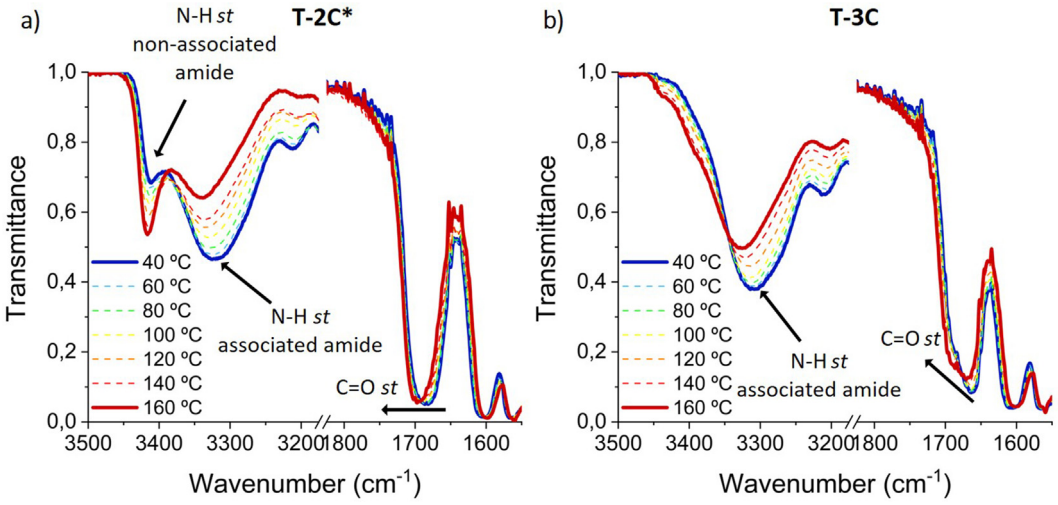

Fig. 7. Infrared spectra of **T-2C*** (a) and **T-3C** (b) at variable temperature.

higher wavenumbers. These results manifest that the transition from the columnar to the cubic phase is gradual, and are consistent with the hypothesis that the formation of spherical micelles occurs from the fragmentation of the columns.

2.2.2.4. Chiroptical properties of LC phases. Electronic circular dichroism (CD) measurements were performed on thin films to analyze a preferential chiral assembly of **T-2C*** in the liquid crystalline state. Linear dichroism artifacts were discarded by recording spectra at different rotation angles of the sample around the light beam (Fig. S19). CD experiments were performed at variable temperature to study the transmission of chirality for both mesophases, i.e. Col_h and BCC. At room temperature, the CD spectrum shows positive and negative bands in the absorption UV/Vis wavelength region of the compound (Fig. 8) consistent with the formation of a columnar mesophase in which chirality is transmitted from the molecule to the stack. The intensity of CD bands remains constant up to 100 °C. The intensity and definition of the CD signal decrease at 160 °C, temperature at which the transition to the isotropic liquid occurs.

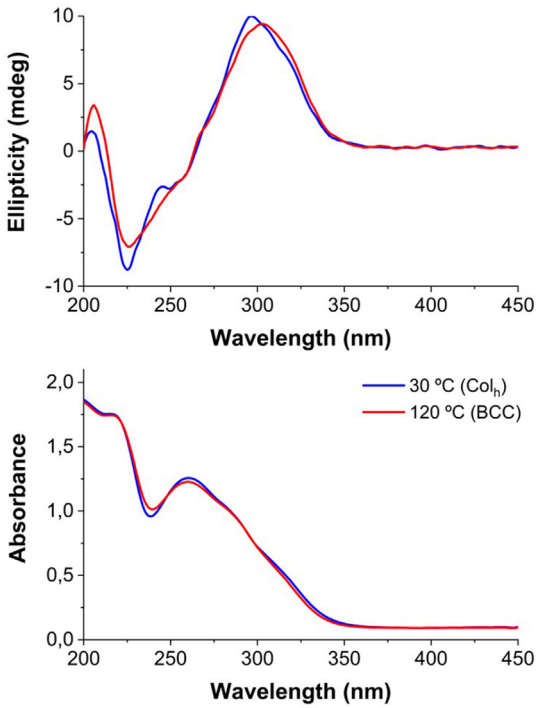

Fig. 8. Circular dichroism at variable temperature and UV/Vis spectra recorded at room temperature for a thin film of **T-2C***.

2.3. Gelation properties

The ability of amide derivatives to form supramolecular polymers stabilized by H-bonding interactions in different media led us to study the self-assembling behaviour of these compounds in organic solvents. The study was carried out at a concentration of 1 wt% in solvents of different polarity, and the results are summarized in Table S1. None of the molecules formed organogels in hydrocarbon solvents, neither aromatic nor aliphatic, and other solvents with different polarity. This failure to self-assemble in solvents agrees with what has been described for star-like C_3-symmetric trisamide oligo(phenylenevinylene) derivatives, for which the formation of organogels in toluene or dodecane is in detriment of liquid crystal behaviour and *vice versa* [36].

Remarkably, all the three compounds are able to gel 1-octanol at concentrations 0.5 to 5 wt% and form opaque gels (Insets of Fig. 9 a-c) with good stability. This behaviour seems incompatible with the presence of amide groups in the molecules, which can compete with 1-octanol for H-bonding interactions, thus disturbing intermolecular H-bonds and the formation of supramolecular fibers that form the gel. Indeed, 1-hexanol has been described as a scavenger that hinders the supramolecular polymerization in dodecane of metalloporphyrin monomers with eight amide groups by competing hydrogen bonding interactions, which impede intermolecular amide-based H-bonds [48]. Interestingly, such competition is not present in our case provided that the tris(triazolyl)triazine core contains H-acceptors that can interact with 1-octanol, similarly to ureidotriazine dimers that admit citronellol as a chiral dopant that does not affect the quadruple H-bonding motif in assemblies of oligo(p-phenylenevinylene) [49]. Hence, 1-octanol is herein proposed to interact orthogonally with the tris(triazolyl)triazine core rather than disturbing intermolecular H-bonds between amide groups. In this situation, the number of alkyl chains around the core increases thus favouring van der Waals interactions that favour self-assembly and gelation. This is supported by the fact that only using hydrocarbon solvents (heptane, dodecane) without the possibility of

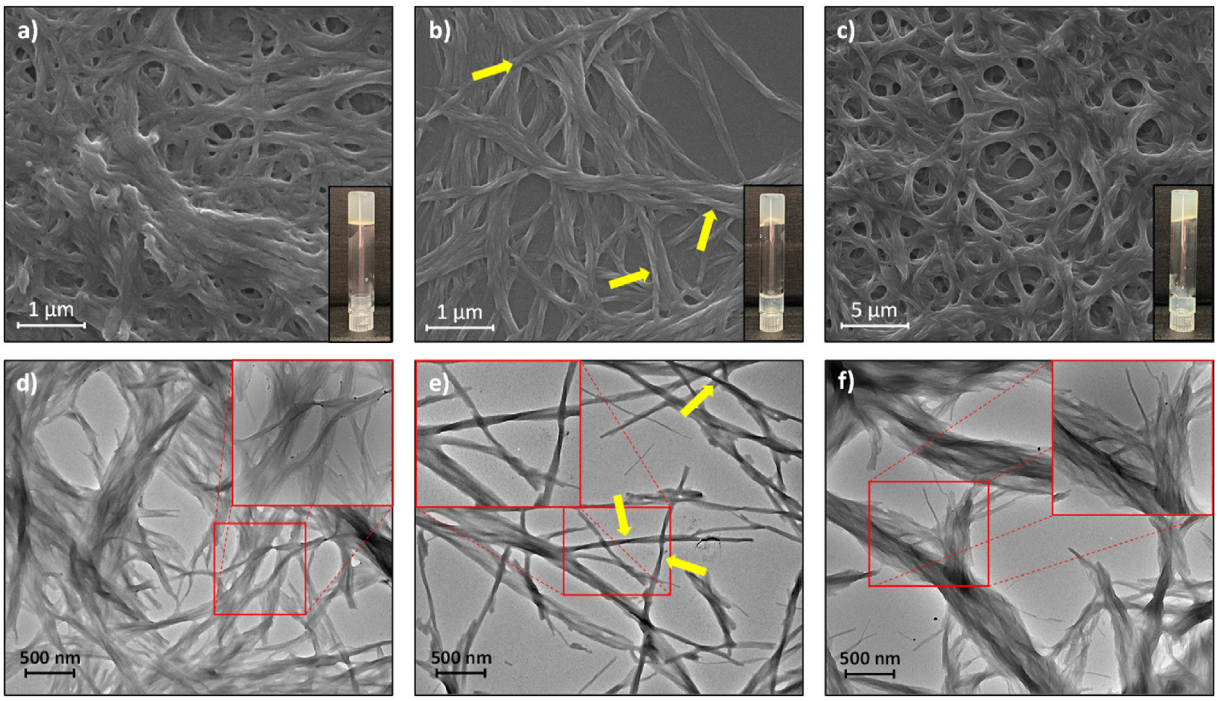

Fig. 9. FE-SEM (top) and TEM (bottom) images of the compounds **T-2C** (a, d), **T-2C*** with left-handed twisted bundles marked with yellow arrows (b, e) and **T-3C** (c, f). The red areas in d-f have been enlarged.

H-bonding interactions with the core does not induce gelation but promote the solution of the molecules.

Compound **T-3C** gels instantaneously whereas the shortest spacer analogues, **T-2C** and **T-2C***, gel more slowly probably because of their incomplete hydrogen bond association. The gel-to-sol transition was estimated to be around 68 °C in compounds **T-3C** and **T-2C** while for the compound **T-2C*** was around 50 °C. This effect is due to the branched spacer that hinders intermolecular interactions yielding less favourable packing, and therefore less stable aggregates [50]. This effect was also observed in the mesophase stability.

The morphology of the xerogels was studied by FE-SEM and TEM (Fig. 9). Xerogel of compound **T-2C** observed by FE-SEM showed a network of entangled fibers whose thickness oscillates between 100 and 250 nm (Fig. 9a,d). TEM images showed that these fibers are made up of thinner fibrils with thickness around 45 nm. FE-SEM and TEM images of compound **T-2C*** exhibit left-handed twisted bundles of fibrils of thickness of about 45 nm which roll up into thicker fibers (Fig. 9b,e). The presence of twists in the fibers could be related with a helical packing of the molecules along the columns that is transmitted to the aggregates. In contrast, FE-SEM observations demonstrated that **T-3C** self-assembles into larger fibers with thickness of about 500 nm that also were constituted by smaller filaments with thickness of 25 nm as observed by TEM (Fig. 9c,f).

2.3.1. X-ray study of gels

Under the POM, all the three gels appeared slightly birefringent (Fig. S20). In order to get more information about the molecular arrangement within the fibers, XRD studies were carried out in gels and their corresponding xerogels. For these studies, gels at concentrations of 5 wt% were employed in order to get reflections of enough intensity to be measured accurately (Fig. 10). In the gel state, compounds **T-2C** (Fig. 10a) and **T-3C** (Fig. 10c) show three reflections in the small angle region. The first two ones can be indexed as reflections 100 and 110 of a hexagonal lattice. The third appears in all the diffractograms as a broad reflection and correspond to a periodic distance of 14.6 Å, which can be related with the longitudinal distance of the solvent molecules. For compound **T-2C***, two reflections that correspond to reflections 100 and 210 of the hexagonal lattice could be observed (Fig. 10b), in addition to a broad reflection of the solvent. These data indicate a hexagonal columnar organisation of the materials in the gel state with *a* parameter values of 47.7 Å for compound **T-2C**, 38.3 Å for compound **T-2C*** and 50.6 Å for compound **T-3C**. As can be observed, both **T-2C** and **T-3C** exhibit an increase of the *a* parameter with respect to that of the mesophase, which could be indicative of the presence of solvent molecules within the column. However, the chiral compound **T-2C*** shows an unexpected decrease that could be related with interdigitation between adjacent homochiral helical columns [20].

In xerogel samples, all compounds show more complex XRD patterns (Fig. 10d–f) consistent with hexagonal lattices. Furthermore, the *a* parameter values are similar to those obtained in the gel state, 46.8 Å for compound **T-2C**, 38.9 Å for compound **T-2C*** and 49 Å for compound **T-3C**. These two facts manifest that gel and xerogel organisation are similar.

2.3.2. FTIR study of xerogels

The study of the intermolecular hydrogen bonds involved in the molecular packing of the gels was carried out by FTIR, and the resulting spectra were compared to these of the mesophase. All the three compounds show N–Hst and C=Ost bands consistent with their involvement in hydrogen bonds (Fig. S21). Compounds **T-2C** and **T-2C*** show a N-Hst band at 3260 cm^{-1} and a C=Ost band centered around 1675 cm^{-1}. Additionally, a small band at 3410 cm^{-1} due to free N–H is visible for **T-2C**. As compared to FTIR spectra in the mesophase (Fig. 7a), these results indicate a more efficient formation of hydrogen bonds between amide groups along the fibres in the gel state than in the mesophase. Compared with its analogues, compound **T-3C** shows a broader N-Hst band centered around 3270 cm^{-1} and a sharp C=Ost band centered around 1660 cm^{-1}, and this is similar to what is observed for the mesophase (Fig. 7b).

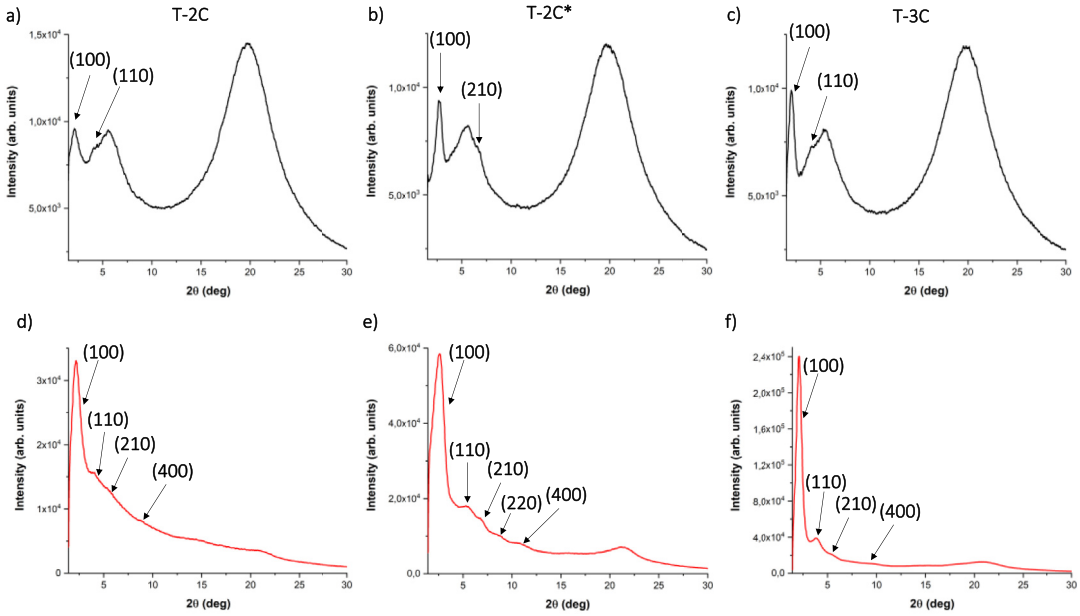

Fig. 10. X-Ray diffractograms of gels in 1-octanol at 5 wt% (top) and the corresponding xerogels (bottom) of compounds **T-2C** (a,d), **T-2C*** (b,e) and **T-3C** (c,f).

2.3.3. *Chiroptical properties of gels*

The chiroptical properties of two gels formed by **T-2C*** in 1-octanol, 1 wt% (Fig. 11 and Figs. S23 and S24a) and 0.5 wt% (Fig. S24b), were studied at room temperature as well as on heating above the gel-to-sol transition. Linear dichroism artifacts were discarded by recording spectra at different positions of the sample (Fig. S23). The overall shape of the CD spectra is in agreement with the existence of chirality in the gel, similarly to that observed in the mesophase (Fig. 8). Nevertheless, an intense bisignate signal with a zero crossing at 259 nm can be observed which was not present in the CD spectra recorded in the mesophase. Interestingly, this bisignate signal corresponds to an absorption maximum originated by the contribution of the π-π* transition of both chromophores present in the molecule, namely the tris(triazolyl)triazine core [24] and the trialkoxyaniline group. We can qualitatively explain this CD signal as the result of the exciton coupling of the corresponding absorptions of these chromophores in close helical disposition, leading to a helical stacking of the molecules within the columns. This model is supported by the columnar arrangement observed in XRD experiments, and by the efficient establishment of intra-columnar hydrogen bonds between amide groups in the gel state, as deduced from FTIR spectra, and which affords effective transmission of the chirality along the columns.

Experiments at variable temperature were performed to study the stability of the chiral aggregates with the temperature. As observed in Fig. S23, the CD intensity decreases drastically at around 50 °C according to the gel-to-sol transition, and this is consistent with the molecular dissolution of the aggregates.

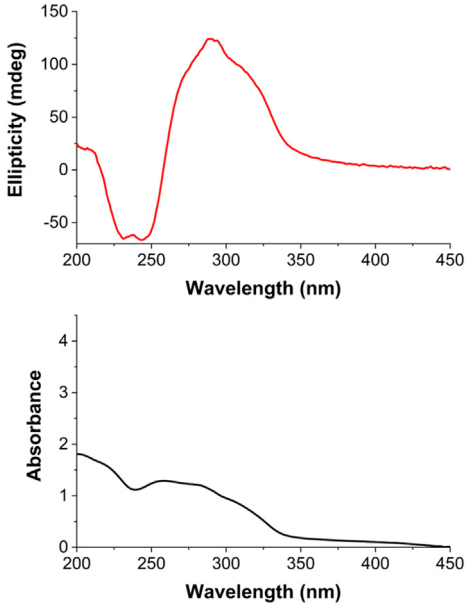

Fig. 11. Circular dichroism (a) and UV/Vis (b) spectra recorded at room temperature for a 1-octanol gel of **T-2C*** (1 wt%).

3. Conclusions

An optimized one-pot CuAAC reaction has enabled the synthesis of three new star-shaped tricarboxamides with C_3 symmetry that have flexible amide spacers linking a tris(triazolyl)triazine core with three trialkoxyphenyl groups. The molecules provide soft materials in bulk and in solvents, the nanostructure of which is stabilized by hydrogen bonding interactions between amide groups.

In bulk, the new molecules present liquid crystalline behavior with thermal properties significantly dependent on the length and linearity of the amide spacer, which also influence the participation of hydrogen bonds. At room temperature, all the compounds display a Col_h phase, which transforms into a cubic phase on heating. This transformation occurs through the division of the columns into small fragments constituted by folded-conformers of the molecule that are arranged in spherical assemblies. Such folded conformers can form thanks to the flexibility of the amide spacer that leads the peripheral trialkoxyphenyl groups to locate at different heights with respect to the plane defined by the core. Accordingly, a supramolecular memory effect, as named by Percec et al. [38], can be proposed to occur in the transformation process between the BCC and the Col_h phase. The variation of the FTIR bands corresponding to the associated N-Hst and C=Ost vibrations

indicates that the transition from the Col_h phase and the cubic phase is gradual, and this supports that the cubic phase is formed by column fragments that form spherical micelles. Interestingly, CD experiments show the effective transmission of chirality form the molecule to both the Col_h and the BCC mesophases, and this constitutes further evidence of the fragmentation of columns in the transition to the BCC phase.

In solvents, all the three compounds are able to gel 1-octanol at low concentrations and form stable opaque gels, which consist on entangled fibers with thicknesses of few tens of nanometers. As deduced from X-ray and FTIR experiments, the arrangement of the molecules resembles what is observed in the mesophase, with the establishment of hydrogen bonds and the formation of a hexagonal columnar organization within the fiber. Furthermore, the transference of chirality confirmed by CD experiments is consistent with a helical stacking of the molecules within the columns.

In summary, this work illustrates the importance and versatility of intermolecular interactions, including π-stacking, van der Waals and hydrogen bonding, to modulate the self-association of C_3-symmetric mesogens in bulk as well as in solvents, thus providing soft materials with defined nanostructures and opening possibilities to include functionalities in the material in a controlled fashion.

Credit author statement

Alejandro Martínez-Bueno: Methodology, Formal analysis, Investigation, Visualization, Writing – original draft.

Raúl Vidal: Methodology, Formal analysis.

Josu Ortega: Methodology, Formal analysis, Visualization, Writing – review & editing.

Jesús Etxebarria: Methodology, Formal analysis, Visualization, Writing – review & editing.

César L. Folcia: Methodology, Formal analysis, Writing – original draft, Writing – review & editing, Funding acquisition.

Raquel Giménez: Conceptualization, Methodology, Writing – review & editing, Project administration, Funding acquisition, Supervision.

Teresa Sierra: Conceptualization, Methodology, Writing – review & editing, Project administration, Funding acquisition, Supervision.

Declaration of competing interest

The authors declare that they have no known competing financial interests or personal relationships that could have appeared to influence the work reported in this paper.

Data availability

Reseach data are included in the supplementary information sent in the Attached files step

Acknowledgements

This work was financially supported by the Spanish projects PGC2018-093761-B-C31, PID2021-122882NB-I00, PID2021-126132NB-I00 MCIN/AEI/10.13039/501100011033/ and by "ERDF A way of making Europe", the Gobierno de Aragón-FSE (E47_20R-research group) and the Basque Goverment (Project IT1458-22). The authors would like to acknowledge the Laboratorio de Microscopias Avanzadas-LMA (Instituto de Nanociencia y Materiales de Aragón-Universidad de Zaragoza), Servicio General de Apoyo a la Investigación-SAI (Universidad de Zaragoza) and Servicios Científico-Técnicos of CEQMA (CSIC- Universidad de Zaragoza) for their support.

Appendix A. Supplementary data

Supplementary data to this article can be found online at https://doi.org/10.1016/j.mtchem.2023.101394.

References

[1] D.V. Talapin, M. Engel, P.V. Braun, Functional materials and devices by self-assembly, MRS Bull. 45 (2020) 799–806.
[2] T. Kato, J. Uchida, T. Ichikawa, T. Sakamoto, Functional liquid crystals towards the next generation of materials, Angew. Chem. Int. Ed. 57 (2018) 4355–4371.
[3] M. Kumar, S. Varshney, S. Kumar, Emerging nanoscience with discotic liquid crystals, Polym. J. 53 (2021) 283–297.
[4] R. De, S. Sharma, S. Sengupta, S. Kumar Pal, Discs to a 'bright' future: exploring discotic liquid crystals in organic light emitting diodes in the era of new-age smart materials, Chem. Rec. 22 (2022), e202200056.
[5] T. Wöhrle, I. Wurzbach, J. Kirres, A. Kostidou, N. Kapernaum, J. Litterscheidt, J.C. Haenle, P. Staffeld, A. Baro, F. Giesselmann, S. Laschat, Discotic liquid crystals, Chem. Rev. 116 (2016) 1139–1241.
[6] M. Lehmann, Star-shaped mesogens – hekates: the most basic star structure with three branches, in: C. Tschierske (Ed.), Liquid Crystals: Materials Design and Self-Assembly, Springer Berlin Heidelberg, Berlin, Heidelberg, 2012, pp. 193–223.
[7] M. Lehmann, Star-shaped mesogens, in: J.W. Goodby, P.J. Collings, T. Kato, C. Tschierske, H. Gleeson, P. Raynes, V. Vill (Eds.), Handbook of Liquid Crystals, vol. 5, Wiley VCH, Weinheim, 2014, pp. 243–315.
[8] E. Beltrán, J.L. Serrano, T. Sierra, R. Giménez, Functional star-shaped tris(-triazolyl)triazines: columnar liquid crystal, fluorescent, solvatofluorochromic and electrochemical properties, J. Mater. Chem. 22 (2012) 7797–7805.
[9] E. Beltrán, M. Garzoni, B. Feringán, A. Vancheri, J. Barberá, J.L. Serrano, G.M. Pavan, R. Giménez, T. Sierra, Self-organization of star-shaped columnar liquid crystals with a coaxial nanophase segregation revealed by a combined experimental and simulation approach, Chem. Commun. 51 (2015) 1811–1814.
[10] S. Nath, S.K. Pathak, J. De, S.K. Pal, A.S. Achalkumar, Star-shaped π-gelators based on oxadiazole and thiadiazoles: a structure–property correlation, Mol. Syst. Des. Eng. 2 (2017) 478–489.
[11] J. De, S.P. Gupta, S. Sudheendran Swayamprabha, D.K. Dubey, I. Bala, I. Sarkar, G. Dey, J.-H. Jou, S. Ghosh, S.K. Pal, Blue luminescent organic light emitting diode devices of a new class of star-shaped columnar mesogens exhibiting π–π driven supergelation, J. Phys. Chem. C 122 (2018) 23659–23674.
[12] N. Tober, T. Rieth, M. Lehmann, H. Detert, Synthesis, thermal, and optical properties of tris(5-aryl-1,3,4-oxadiazol-2-yl)-1,3,5-triazines, new star-shaped fluorescent discotic liquid crystals, Chem. Eur J. 25 (2019) 15295–15304.
[13] B. Mu, X. Quan, Y. Zhao, X. Li, W. Tian, Fluorophore core-engineered supramolecular discotic columnar liquid crystals with tunable fluorescent behavior, Mater. Chem. Front. 3 (2019) 1671–1677.
[14] M. Lambov, N. Hensiek, A.-C. Pöppler, M. Lehmann, Columnar liquid crystals from star-shaped conjugated mesogens as nano-reservoirs for small acceptors, ChemPlusChem 85 (2020) 2219–2229.
[15] B. Mu, Y. Zhao, X. Li, X. Quan, W. Tian, Enhanced conductivity and thermochromic luminescence in hydrogen bond-stabilized columnar liquid crystals, ACS Appl. Mater. Interfaces 12 (2020) 9637–9645.
[16] S. Bujosa, E.E. Greciano, M.A. Martínez, L. Sánchez, B. Soberats, Unveiling the role of hydrogen bonds in luminescent N-annulated perylene liquid crystals, Chem. Eur J. 27 (2021) 14282–14286.
[17] S. Cantekin, T.F.A. de Greef, A.R.A. Palmans, Benzene-1,3,5-tricarboxamide: a versatile ordering moiety for supramolecular chemistry, Chem. Soc. Rev. 41 (2012) 6125–6137.
[18] Y. Dorca, E.E. Greciano, J.S. Valera, R. Gómez, L. Sánchez, Hierarchy of asymmetry in chiral supramolecular polymers: toward functional, helical supramolecular structures, chem, Eur. J. 25 (2019) 5848–5864.
[19] F. García, P.A. Korevaar, A. Verlee, E.W. Meijer, A.R.A. Palmans, L. Sánchez, The influence of π-conjugated moieties on the thermodynamics of cooperatively self-assembling tricarboxamides, Chem. Commun. 49 (2013) 8674–8676.
[20] S. Díaz-Cabrera, Y. Dorca, J. Calbo, J. Aragó, R. Gómez, E. Ortí, L. Sánchez, Hierarchy of asymmetry at work: chain-dependent helix-to-helix interactions in supramolecular polymers, Chem. Eur J. 24 (2018) 2826–2831.
[21] T. Kim, T. Mori, T. Aida, D. Miyajima, Dynamic propeller conformation for the unprecedentedly high degree of chiral amplification of supramolecular helices, Chem. Sci. 7 (2016) 6689–6694.
[22] J.A. Berrocal, F. Di Meo, M. García-Iglesias, R.P.J. Gosens, E.W. Meijer, M. Linares, A.R.A. Palmans, Consequences of conformational flexibility in hydrogen-bond-driven self-assembly processes, Chem. Commun. 52 (2016) 10870–10873.
[23] D. Miyajima, F. Araoka, H. Takezoe, J. Kim, K. Kato, M. Takata, T. Aida, Ferroelectric columnar liquid crystal featuring confined polar groups within core-shell architecture, Science 336 (2012) 209–213.
[24] E. Beltrán, J.L. Serrano, T. Sierra, R. Giménez, Tris(triazolyl)triazine via click-chemistry: a C3 electron-deficient core with liquid crystalline and luminescent properties, Org. Lett. 12 (2010) 1404–1407.
[25] M. Castillo-Vallés, E. Beltrán, J. Cerdá, J. Aragó, P. Romero, J.L. Serrano, E. Ortí, R. Giménez, T. Sierra, Self-assembly of clicked star-shaped triazines into functional nanostructures, ChemNanoMat 5 (2019) 130–137.

[26] M. Peterca, M.R. Imam, C.-H. Ahn, V.S.K. Balagurusamy, D.A. Wilson, B.M. Rosen, V. Percec, Transfer, amplification, and inversion of helical chirality mediated by concerted interactions of C3-supramolecular dendrimers, J. Am. Chem. Soc. 133 (2011) 2311–2328.
[27] M. Lehmann, M. Jahr, Programming star-mesogens toward the formation of columnar or cubic phases, Chem. Mater. 20 (2008) 5453–5456.
[28] C.H.M. Weber, F. Liu, X.-b. Zeng, G. Ungar, N. Mullin, J.K. Hobbs, M. Jahr, M. Lehmann, Body-centered cubic phase in 3-arm star mesogens: a torsional tapping AFM and GISAXS study, Soft Matter 6 (2010) 5390–5396.
[29] D. Sahoo, M. Peterca, E. Aqad, B.E. Partridge, P.A. Heiney, R. Graf, H.W. Spiess, X. Zeng, V. Percec, Hierarchical self-organization of perylene bisimides into supramolecular spheres and periodic arrays thereof, J. Am. Chem. Soc. 138 (2016) 14798–14807.
[30] V. Percec, M.R. Imam, M. Peterca, D.A. Wilson, P.A. Heiney, Self-assembly of dendritic crowns into chiral supramolecular spheres, J. Am. Chem. Soc. 131 (2009) 1294–1304.
[31] M. Castillo-Vallés, A. Martínez-Bueno, R. Giménez, T. Sierra, M.B. Ros, Beyond liquid crystals: new research trends for mesogenic molecules in liquids, J. Mater. Chem. C 7 (2019) 14454–14470.
[32] V. Iguarbe, P. Romero, J. Barberá, A. Elduque, R. Giménez, Dual liquid Crystalline/Gel behavior with AIE effect promoted by Self-assembly of pyrazole dendrons, J. Mol. Liq. 365 (2022), 120109.
[33] H. Cheng, H. Gao, T. Wang, M. Xia, X. Cheng, Polycatenar bent-shaped liquid crystals with columnar and cubic phases: synthesis multi-responsive organogels and chemosensors, J. Mol. Liq. 249 (2018) 723–731.
[34] M. Martínez-Abadía, S. Varghese, J. Gierschner, R. Giménez, M.B. Ros, Luminescent assemblies of pyrene-containing bent-core mesogens: liquid crystals, π-gels and nanotubes, J. Mater. Chem. C 10 (2022) 12012–12021.
[35] S.K. Pathak, B. Pradhan, R.K. Gupta, M. Gupta, S.K. Pal, A.S. Achalkumar, Aromatic π–π driven supergelation, aggregation induced emission and columnar self-assembly of star-shaped 1,2,4-oxadiazole derivatives, J. Mater. Chem. C 4 (2016) 6546–6561.
[36] A. Sandeep, V.K. Praveen, D.S. Shankar Rao, S. Krishna Prasad, A. Ajayaghosh, Transforming a C3-symmetrical liquid crystal to a π-gelator by alkoxy chain variation, ACS Omega 3 (2018) 4392–4399.
[37] T. El Malah, H.F. Nour, A.A. Nayl, R.A. Elkhashab, F.M.E. Abdel-Megeid, M.M. Ali, Anticancer evaluation of tris(triazolyl)triazine derivatives generated via click chemistry, Aust. J. Chem. 69 (2016) 905–910.
[38] J. Barberá, R. Giménez, N. Gimeno, M. Marcos, M.D.C. Pina, J.L. Serrano, Bis(-salicylaldiminate) copper(II) and palladium(II) complexes: towards columnar mesophases, Liq. Cryst. 30 (2003) 651–661.
[39] C. Courme, S. Gillon, N. Gresh, M. Vidal, C. Garbay, J.-C. Florent, E. Bertounesque, Terminal alkyne-functionalized triazine by Sonogashira coupling: synthesis of a potential cell signalling inhibitor via click chemistry, Tetrahedron Lett. 49 (2008) 4542–4545.
[40] M. Zhao, J. Li, E. Mano, Z. Song, D.M. Tschaen, E.J.J. Grabowski, P.J. Reider, Oxidation of primary alcohols to carboxylic acids with sodium chlorite catalyzed by TEMPO and bleach, J. Org. Chem. 64 (1999) 2564–2566.
[41] B. Pal, P. Jaisankar, V.S. Giri, Versatile reagent for reduction of azides to amines, Synth. Commun. 34 (2004) 1317–1323.
[42] G. Ungar, F. Liu, X. Zeng, Cubic and other 3D thermotropic liquid crystal phases and quasicrystals, in: Handbook of Liquid Crystals, 2014, pp. 1–74.
[43] B. Feringán, J. Cerdá, B. Diosdado, J. Aragó, E. Ortí, R. Giménez, T. Sierra, On the structure and chiral aggregation of liquid crystalline star-shaped triazines H-bonded to benzoic acids, Chem. Eur J. 26 (2020) 15313–15322.
[44] M. Peterca, M.R. Imam, S.D. Hudson, B.E. Partridge, D. Sahoo, P.A. Heiney, M.L. Klein, V. Percec, Complex arrangement of orthogonal nanoscale columns via a supramolecular orientational memory effect, ACS Nano 10 (2016) 10480–10488.
[45] D. Sahoo, M. Peterca, E. Aqad, B.E. Partridge, P.A. Heiney, R. Graf, H.W. Spiess, X. Zeng, V. Percec, Tetrahedral arrangements of perylene bisimide columns via supramolecular orientational memory, ACS Nano 11 (2017) 983–991.
[46] N. Huang, M.R. Imam, M.J. Sienkowska, M. Peterca, M.N. Holerca, D.A. Wilson, B.M. Rosen, B.E. Partridge, Q. Xiao, V. Percec, Supramolecular spheres assembled from covalent and supramolecular dendritic crowns dictate the supramolecular orientational memory effect mediated by Frank–Kasper phases, Giant 1 (2020), 100001.
[47] A. Desmarchelier, B.G. Alvarenga, X. Caumes, L. Dubreucq, C. Troufflard, M. Tessier, N. Vanthuyne, J. Idé, T. Maistriaux, D. Beljonne, P. Brocorens, R. Lazzaroni, M. Raynal, L. Bouteiller, Tuning the nature and stability of self-assemblies formed by ester benzene 1,3,5-tricarboxamides: the crucial role played by the substituents, Soft Matter 12 (2016) 7824–7838.
[48] K. Venkata Rao, D. Miyajima, A. Nihonyanagi, T. Aida, Thermally bisignate supramolecular polymerization, Nat. Chem. 9 (2017) 1133–1139.
[49] S.J. George, Ž. Tomović, A.P.H.J. Schenning, E.W. Meijer, Insight into the chiral induction in supramolecular stacks through preferential chiral solvation, Chem. Commun. 47 (2011) 3451–3453.
[50] S. Moyano, J.L. Serrano, A. Elduque, R. Giménez, Self-assembly and luminescence of pyrazole supergelators, Soft Matter 8 (2012) 6799–6806.